ACS Photonics

pubs.acs.org/journal/apchd5 Article

Angle- and Polarization-Independent Structural Color Based on Controlled Phase and Gain Margins in Ultrathin Transparent Dielectrics

Pablo Cencillo-Abad, Sean McCormack, Tianyi Guo, Aritra Biswas, and Debashis Chanda*

Cite This: https://doi.org/10.1021/acsphotonics.3c00632 Read Online

ACCESS | Metrics & More | Article Recommendations | Supporting Information

ABSTRACT: Fascination with nature's color palette has propelled mankind's efforts to imitate and surpass it. Apart from the traditional interests in brighter and more fade-resistant colors, the present time adds the need for doing so without impacting the environment based on nontoxic materials. Although most commercial colorants are based on chemical pigments that absorb wavelengths of light matching their electronic and molecular transitions, the development of nanofabrication techniques in the last decades has spurred researchers to study structural colors, where color can be made out of colorless materials by carefully designed micrometer and nanoscale inclusions. Although, a myriad of such configurations have been reported for the production of color, in most cases, they suffer from angle or polarization dependence or require expensive materials or impractical fabrication techniques that are incompatible with large-scale production. Recently, some approaches have been proposed for the use of random media to mitigate these effects. Here, we demonstrate an approach based on colorless mirrors and transparent lossless dielectrics and show how this can be harnessed to produce a full color palette by using a subwavelength bilayer structure composed of thin films of titanium and its oxide for the production of inexpensive structural color. Furthermore, we introduce an additive manufacturing process that creates 58 different hues from 4 primaries in only three sequential evaporations. Based on this color palette, we reproduce Van Gogh's self-portrait on a 1 sq in. area providing proof of the applicability of the platform for large-scale, low-cost, and environmentally friendly production of structural colors.

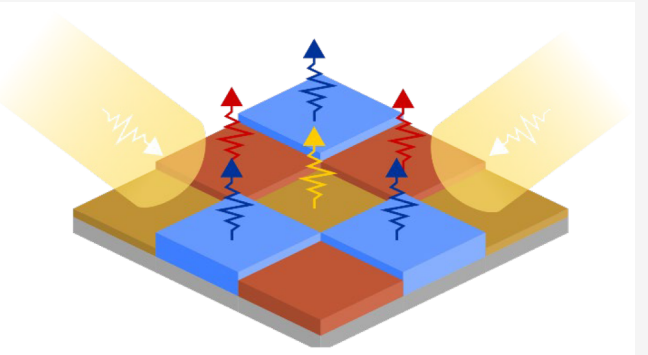

KEYWORDS: *structural color, phase gain margin, ultrathin optical cavities, functional nanocoatings*

INTRODUCTION

We live in a world of color. Colors signal actions, evoke feelings, and offer vital information about our surroundings. Fascination with nature's color palette has propelled mankind's efforts to imitate it: from the primitive mixtures of minerals, ashes, and organic components of the cavemen 40000 years ago, to reach the modern industrial production of acrylic paints.[1] Indeed, it can be said that the history of color production is the history of art, culture, and humanity.[2] Modern day has added to the traditional quest of finding brighter and more resistant colorants, with a special emphasis in doing it based on nontoxic materials to save the environment.[3−5]

For nonluminous objects, colorants, substances used to impart color, are used to either absorb or reflect specific spectral components of the incoming light. Color is thus the result of these constituent's interaction with the external illumination, and controlling it selectively allows one to tailor the color appearance of an object. Coloration mechanisms have been divided in two broad categories: chemical or pigment-based coloration; and physical or structural-based coloration.[6] Commercial colorants are based on chemical compounds that absorb specific wavelengths of light matching their electronic and molecular transitions.[5] In this manner, commercial paints impart color by removing certain bands from the illuminating white light and reflecting the rest. Being chemically synthesized, these colorants offer a route for large scale and low-cost production, both essential for commercial production.[7−9] However, they suffer from chemical instability that results in premature fading, require coatings of several 100s of micrometers to millimeter to impart full coloration, and their synthesis often times requires toxic materials or contaminant methods that harm the environment.[5,10]

Received: May 12, 2023

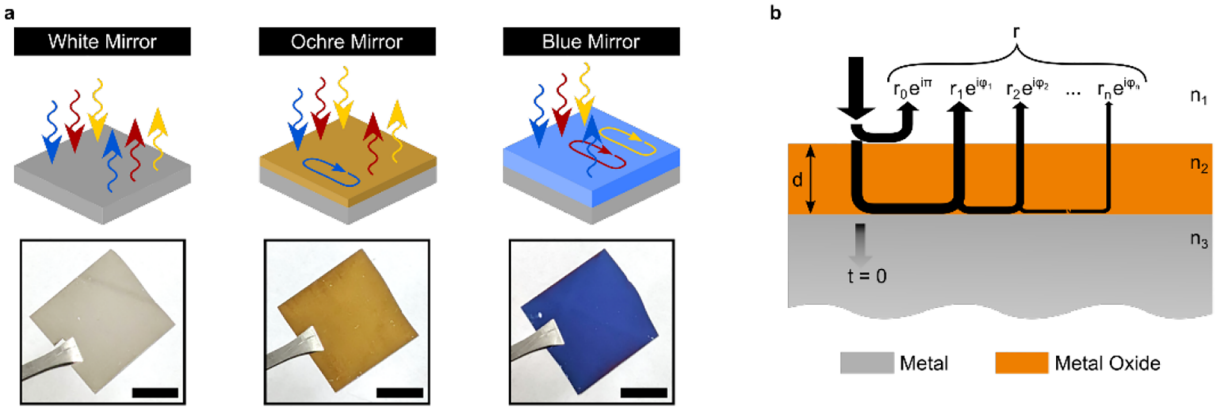

Figure 1. Coloring colorless metals with ultrathin transparent dielectrics. (a) Colorless metals such as silver or titanium reflect relatively evenly all components of the visible light (left). However, coating with a transparent dielectric layer of specific thickness can result in enhanced absorption of specific spectral bands and thus color appearance (center and right). Scale bar: 1.5 cm. (b) The color appearance is the result of the destructive interference of the multiple reflected beams that occurs propagating in the cavity. For a given combination phase and amplitude are matched to absorb certain wavelengths.

Although structural color has been studied for a long time, the widespread development of nanofabrication techniques in the last decades has spurred a renewed interest.[11−15] By engineering the geometry of an object, researchers can harness physical phenomena such as scattering, interference, or diffraction to carefully tailor its color appearance based on colorless materials.[8,16−19] Typically, structural colors offer brighter metallic-like shades, long-term stability, and environmental friendliness.[8,16−19] Nevertheless, to date, only Lexus Blue by Toyota[20] has found successful use in large-scale production. Indeed, to bridge the gap from proof-of-principle to industrial production, some challenges still need to be addressed. In particular, many structural colors lack practicality as they suffer from angle or polarization dependency, or require expensive materials or nonversatile fabrication methods, resulting in very costly designs that cannot be exploited commercially.[18,21−23]

One of the simplest methods to create structural colors is based on the use of interferometers comprising two reflective surfaces spaced by either a stack or a thin transparent dielectric.[24] This configuration, known as a Fabry−Perot resonator, exploits constructive and destructive interference of beams to suppress and enhance some spectral bands at specific wavelengths matching the resonance of the cavity.[25,26] Interestingly, as it is a purely geometric effect, the color of these Fabry−Perot resonators can be easily tuned by changing the thickness of the spacer layer. In recent years, researchers have exploited noble metals, liquid crystals, phase-change materials, semiconductors, and high-reflective index materials to produce such structural color.[24,27−40] However, the use of many of these comes at the expense of angle dependency, cost of materials or require nanofabrication techniques not scalable for industrial production.[41]

Recently, we demonstrated a structural color based on self-assembled aluminum nanoparticles that harnesses the randomness of the plasmonic layer to produce simultaneous angle and polarization independence.[42] Here, we report another straightforward and inexpensive platform for structural color that uses a bilayer architecture of titanium and its oxide to produce a gamut of polarization and angle-insensitive colors. The stack is formed by growing on top of a back-reflecting mirror a thin layer of its transparent oxide. In contrast to conventional architectures, that accumulate phases solely in the dielectric layer, the inclusion of a lossy mirror allows for nontrivial phases to occur at the dielectric−mirror interface. The phase introduced, combined with the amplitude modulation resulting from the intrinsic losses of the lossy mirror, suffices to produce full-coloration with a bilayer structure, thus significantly reducing the complexity of the architecture and the fabrication demands. Importantly, in a manner analogous to phase- and margin gain control for system stability, the particular combination of the losses and phases at the oxide/metal interface relaxes the requirements for the geometry, resulting in a robust angle-independent resonance for very thin dielectrics. In this work, we analyze the material requirements and theoretical conditions for producing such inexpensive structural colors. Furthermore, we introduce an additive structural color mixing process that creates 58 different hues from only 4 primaries that are grown from the same materials, thus enormously simplifying the fabrication costs. Finally, following this process, we reproduce a self-portrait paint by Vincent Van Gogh on a 1 sq in. area providing further proof of the applicability of the platform for large-scale fabrication.

RESULTS

Colored Colorless-Mirror with Ultrathin Transparent Dielectric. Fabry−Perot cavities harness the interference pattern of multiple beams reflecting at two interfaces to enhance the absorption or reflection of light at specific wavelengths. This high-resolution and versatile architecture is found at the core of many optoelectronic systems in telecommunications, lasers, or spectroscopy.[43,44] These optical cavities form a closed-loop system that displays great instability with even small angle variation. This behavior, arising from its pure geometrical nature, greatly limits their use in coloration applications. Here, we analyze how controlling the phase and gain margins of an optical system consisting of a lossy optically thick mirror coated by a thin layer of its transparent oxide, Figure 1a, one can achieve full-coloration while enormously reducing the angle dependency.

In contrast to colored metals such as copper or gold; metals such as silver, aluminum, chromium, or titanium appear colorless when illuminated with white light. Having their

https://doi.org/10.1021/acsphotonics.3c00632
ACS Photonics XXXX, XXX, XXX−XXX

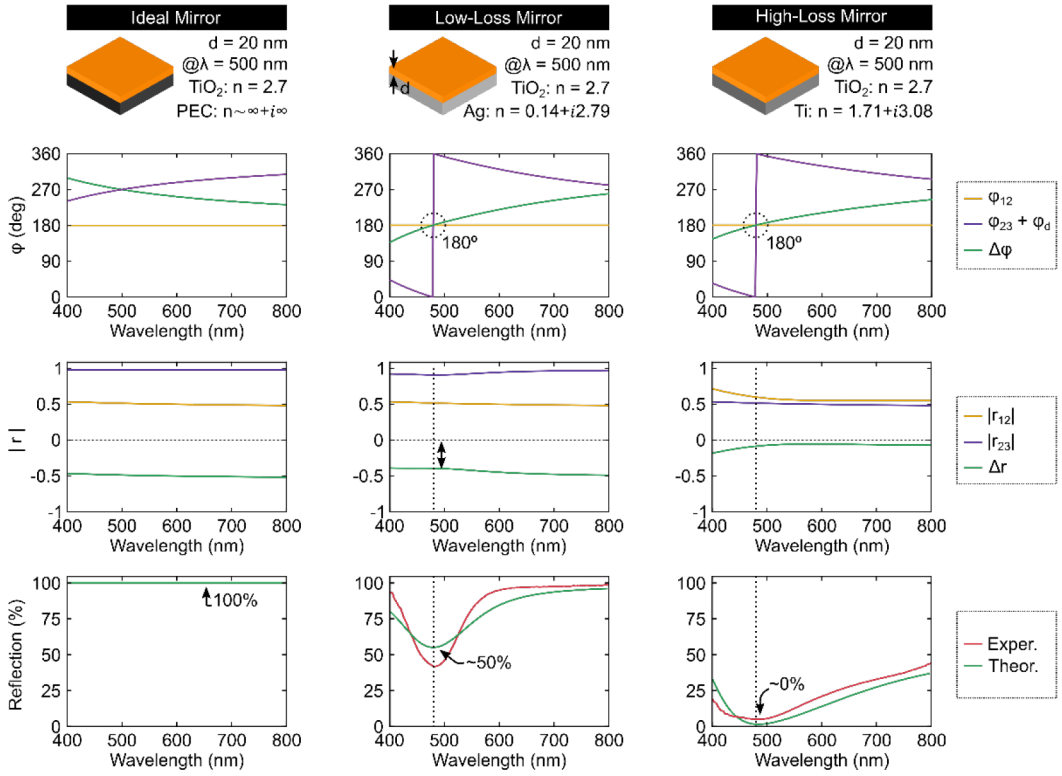

Figure 2. Optical conditions for reflection suppression with lossless dielectrics. We examine theoretically the phase (first row) and amplitude (second row) conditions necessary for suppressing reflection (third row) on three mirror substrates coated with a 20 nm TiO_2 layer. The first column corresponds to an ideal mirror (PEC), the second column represents a highly reflective mirror (Ag), and the third column pertains to a lossy mirror (Ti). For the reflection curves, the theoretical prediction (green curve) is compared to the experimentally measured samples (green curve), demonstrating a good agreement between them.

plasma frequencies in the UV, these colorless metals reflect relatively evenly all the wavelengths of visible light, with different shades of gray resulting from the different amount of intrinsic losses that the materials present: from the light-gray of silver or aluminum (over 90% reflection across the visible spectrum), to darker shades of gray corresponding to titanium or chromium (∼60% reflection across the visible spectrum).[45] However, if the metallic film is coated with a thin layer of a certain thickness of a transparent dielectric, the resonance condition of the cavity is fulfilled and the stack shows a bright color, if the cavity phase and gain margins are met. The particular wavelengths at which this phenomenon occurs are ultimately determined by the material properties of the multilayer and the geometry of the cavity. To analyze these conditions, we consider first the general case with a three-layer system consisting of a dielectric of thickness d and refractive index n_2, sandwiched by two semi-infinite layers of air ($n_1 = 1$) on top, and metal (n_3) on bottom. When a beam of light impinges on the first interface, part of the light will be back reflected while the other will be transmitted into the cavity. After passing through the dielectric accumulating a phase, this beam will be subsequently partially reflected back and forth between the two interfaces (dielectric/metal and dielectric/air), generating multiple beams, Figure 1b. Adding the amplitude of all these successive rays we can finally obtain the overall reflection coefficient of the stack:[46]

$$r = \frac{r_{12} + r_{23}e^{i2\varphi}}{1 + r_{12}r_{23}e^{i2\varphi}} \tag{1}$$

where r_{ij} denotes the Fresnel coefficient for the reflection from layer i to layer j; and φ denotes the phase factor that accounts for the geometric path difference between any two successive beams that cross twice the dielectric layer:

$$\varphi = n_2 \frac{2\pi d}{\lambda} \cos\theta_2 \tag{2}$$

where λ is the wavelength of the beam and θ_2 is the refracted angle that can be found from Snell's law. Finally, the total reflection of the system is simply computed as $R = |r^2|$.

In general, for suppressing the reflection, the numerator of eq 1 needs to be zero. However, in contrast to lossless materials, where the refractive index is purely real, for lossy media, the refractive index function takes complex values. Consequently, the Fresnel coefficients will also be complex and the condition of zero reflection will be matched whenever:

$$\begin{cases} |r_{12}| = |r_{23}|e^{-\mathrm{Im}\{n_2\}4\pi d/\lambda \cos\theta_2} \\ \varphi_{12} + \varphi_{23} + 2\varphi_{\mathrm{prop}} = 2m\pi \end{cases} \tag{3}$$

with m being an integer and $\varphi_{\mathrm{prop}} = \frac{2\pi d}{\lambda}\mathrm{Re}\{n_2\}\cos\theta_2$ being the propagation phase accumulated through the dielectric layer. The first condition can be interpreted as an amplitude matching condition: amplitude of the beams need to be the same to cancel, and to achieve this, one needs to consider not only the amplitude of the reflections at the interfaces but also the losses in the dielectric during propagation. On the other hand, the second condition refers to the phase condition expected for achieving destructive interference.

https://doi.org/10.1021/acsphotonics.3c00632
ACS Photonics XXXX, XXX, XXX−XXX

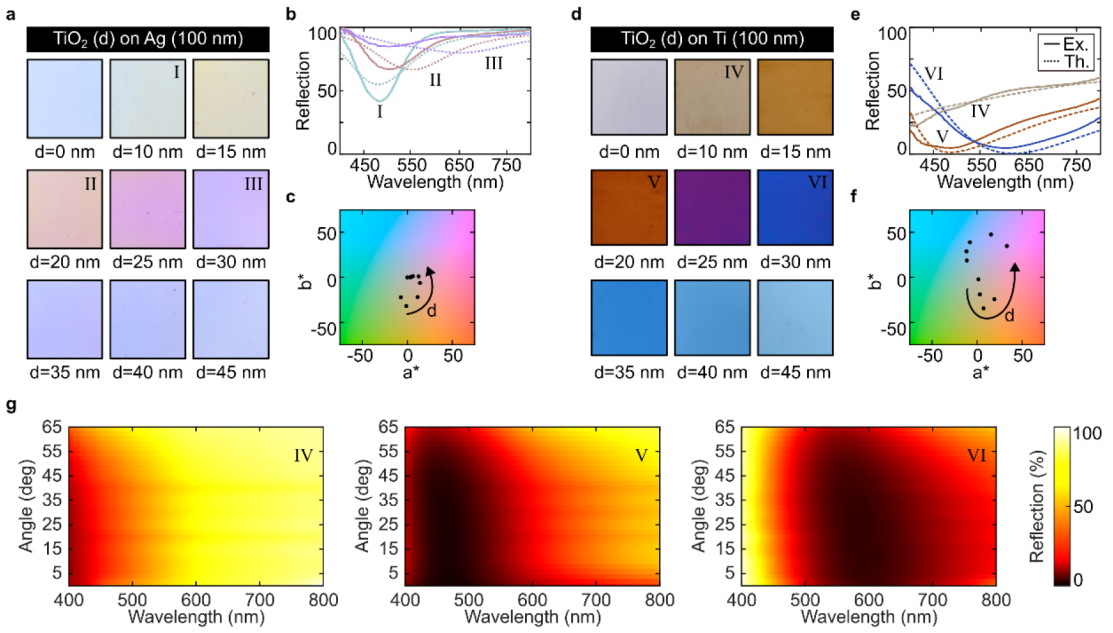

Figure 3. Color palette for low- and high-loss reflective mirrors. Photographies of the colors produced when coating silver (a) and titanium (d) mirrors with thin layers of titanium dioxide ranking from 10 to 45 nm in steps of 5 nm. (b, e) Three samples' reflection curves corresponding to 10 (I and IV), 20 (II and V), and 30 nm (III and VI) thick titanium dioxide layers on top of silver (b) and titanium (e) mirrors. Experimental curves (solid lines) are recorded at normal incidence and show good agreement with the theoretical prediction (dotted line). (c, f) CIELAB coordinates for silver (c) and titanium (f) samples. (g) Thin layers of dielectric employed result in great angle-independency colors. Titanium mirrors coated with 10 (yellow), 20 (magenta), and 30 nm (cyan) TiO_2 show great angle-independency up to 65°.

To gain further physical insight, it is convenient to study analytically the case of normal incidence ($\theta_1 = \theta_2 = 0$). For $n_1 < n_2 < n_3$, in the absence of losses, the refractive indices will be real values and the phases of the reflections at the interfaces will be simply $\varphi_{12} = \varphi_{23} = \pi$. Thus, the destructive interference will happen only whenever the phase accumulated through propagation is an odd multiple of $\pi/2$, which solves for the thickness of the dielectric layer yields

$$d = \frac{2m\lambda}{4n_2} + \frac{\lambda}{4n_2}$$

For antireflection coatings typically $m = 0$, and hence, from conservation of energy, when no absorption is present, all the energy is transmitted ($T = 1 - R$). However, when the back-mirror is optically thick, no transmission can happen ($T = 0$), and all the radiation needs to be fully reflected. This imposes an important physical condition: to achieve full suppression of a given spectral wavelength, in the absence of transmission, all the radiation needs to be absorbed, and this can only happen either at the mirror or the dielectric layer. A critical result follows from this observation. As we have seen, when absorption is present, the Fresnel coefficients are complexed valued. Therefore, the phases gained upon reflection at the interfaces (φ_{12},φ_{23}) can take nontrivial values from 0 to 2π. This opens a new route for phase matching that does not depend only on the dielectric length but also on the particular materials used.

To further analyze the consequences of these results, we will study the matching conditions for three mirrors: an ideal perfect electric conductor (PEC, $n_3 = \infty + i\infty$), a low-loss mirror (silver), and a lossy mirror (titanium); coated by a 20 nm layer of a lossless transparent dielectric (titanium dioxide). While titanium oxide is chosen as the native oxide of the bottom titanium back mirror due to its integration advantages, it is important to note that any transparent dielectric can lead to coloration as long as the phase and amplitude conditions are met. The phases and amplitude components and the overall reflection for all three stacks at visible wavelengths can be seen in Figure 2. Values are calculated with MATLAB from the analytical equations for the normal incidence. The refractive index for titanium dioxide is experimentally determined (Filmetrics F40) to be constant with value $n_2 = 2.7$, whereas the dispersive refractive indices of titanium and silver are taken from literature.[47] The first row in Figure 2 reflects the phase matching condition of eq 3. In all three configurations, the phase at the air/oxide interface (φ_{12}, yellow curve) will be π. Hence, to match the phase condition, the sum of twice the propagation phase and the reflection at the oxide/mirror interface (purple curve) needs to be an odd multiple of π. The second row shows the comparison of amplitudes for all three configurations. In this case, for the condition to be fulfilled, both amplitudes $|r_{12}|$ (yellow curve) and $|r_{23}|$ (purple curve) need to be equal. Finally, the last row shows the total reflection curve ($R = |r^2|$ (green curve)). Overlaid with the theoretical curve, we plot the experimentally measured reflection for two fabricated samples (red curve) of silver and titanium mirrors coated with 20 nm of titanium dioxide. Reflection measurements were taken at normal incidence with unpolarized light using a 4×, 0.07 numerical aperture objective and a fiber coupled spectrometer (HR 2000+, Ocean Optics).

As expected, in the case of the PEC mirror, when neither absorption nor transmission can occur, all light is reflected (first column). In this configuration, known as a Gires–Tournois, all light is reflected with an overall phase shift. On the other hand, when comparing the cases of silver and titanium mirror (second and third columns), an interesting fact is observed. Even though both match the phase margin, only the titanium mirror cavity is close enough to fulfill the gain

https://doi.org/10.1021/acsphotonics.3c00632
ACS Photonics XXXX, XXX, XXX−XXX

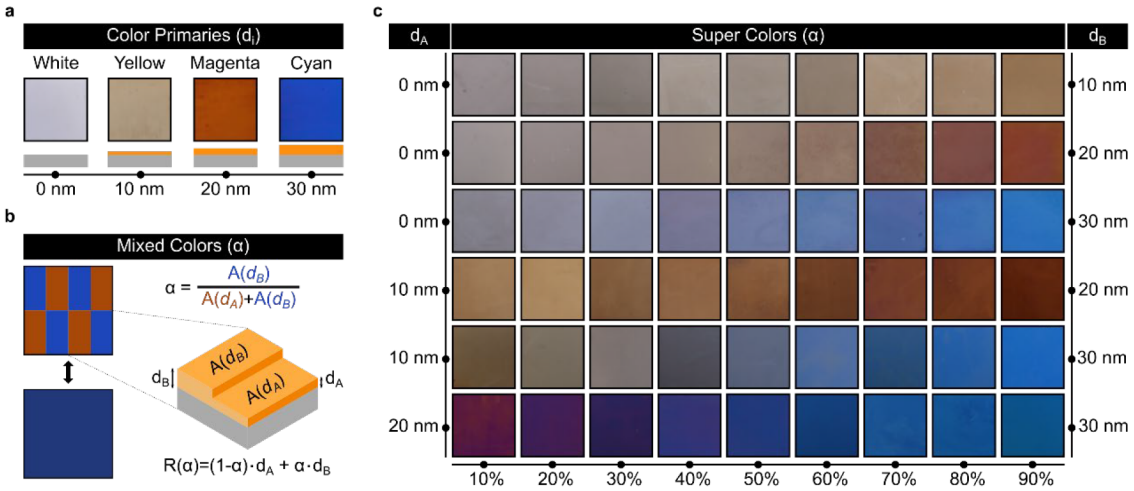

Figure 4. Expanding the color palette. (a) Only four color primaries corresponding to white (no coating), yellow (10 nm), magenta (20 nm), and cyan (30 nm) are required to produce a full color space. (b) By mixing two primaries in different proportions of the covered area over the total area, α, the color palette can be expanded. The reflection of the composite configuration, arranged in a chessboard to reduce color aliasing (inset), is given by a simple weighted addition rule. (c) Photographs of all combinations corresponding to mixing ratios from 0 to 100% every 10%.

margin. Hence, whereas for the titanium mirror a band in the neighborhood of 490 nm is almost completely suppressed and a saturated color is apparent, the mismatch in amplitudes for the silver cavity results in partially destructive interference, weak resonance excitation, and less saturated colors.

Color Production from Low- and High-Lossy Mirrors. To further investigate the contrast in color production for highly reflective and lossy mirrors, we evaporate (Thermionics) on microscope slides 9 silver and 9 titanium optically thick mirrors. Each of the mirrors is then subsequently coated with 10 to 45 nm titanium dioxide in steps of 5 nm. As expected, while the lossy titanium produces near perfect absorption and thus saturated colors, the silver mirror only results in pale and dull tints. The pictures of the samples are shown in Figure 3a,d. The difference in color contrast is purely due to the intrinsic losses of the mirror layer and is in good agreement with previous conclusions. For full reflection suppression both amplitude and phase need to match, but for a lossless dielectric, this can only happen when losses are introduced through the mirror. Indeed, for samples fabricated with a selection of different high and low reflection mirrors (for instance aluminum and chromium, respectively), the same effect is observed (see Supporting Information, Figure S1). The difference in color contrast between high- and low-loss configurations can be also seen in the reflection curves, Figure 3b,e. While coated-titanium mirrors reach almost zero reflection at specific bands, the silver samples show reflection levels consistently over 50% at the resonances. This lack of saturation in the colors is better appreciated in the CIELAB plots shown in Figure 3c,f. The titanium mirror samples (top) show better contrast than the silver mirror (bottom), offering additionally a larger color space. To obtain the CIELAB components of each of the samples, we first obtain the *XYZ* tristimulus values integrating over the visible spectrum according to

$$X = \frac{1}{N}\int \bar{x}(\lambda)R(\lambda)I(\lambda)\,\mathrm{d}\lambda$$

$$Y = \frac{1}{N}\int \bar{x}(\lambda)R(\lambda)I(\lambda)\,\mathrm{d}\lambda$$

$$Z = \frac{1}{N}\int \bar{x}(\lambda)R(\lambda)I(\lambda)\,\mathrm{d}\lambda$$

$$N = \int \bar{y}(\lambda)I(\lambda)\,\mathrm{d}\lambda$$

where $R(\lambda)$ is the measured reflectance; $\bar{x}(\lambda)$, $\bar{y}(\lambda)$, and $\bar{z}(\lambda)$ are the color matching functions; $I(\lambda)$ is the reference illuminant. From the tristimulus values CIEXYZ, the CIELAB coordinates can be calculated from

$$L^* = 116f_y - 16$$

$$a^* = 500(f_x - f_y)$$

$$b^* = 200(f_y - f_z)$$

where being $t_x = \frac{X}{X_n}$, $t_y = \frac{Y}{Y_n}$, or $t_z = \frac{Z}{Z_n}$; and $X_N = 0.9642$, $Y_N = 1.0000$, and $Z_N = 0.8251$ the D50 white point coordinates:

$$f_i = \begin{cases} \sqrt[3]{t_i} & \text{if } t > \left(\frac{6}{29}\right)^3 \\ \frac{841t_i}{108} + \frac{4}{29} & \text{otherwise} \end{cases}$$

We selected D50 as the reference illuminant, the one used in the graphic arts industry for color proofing (ISO 3664:2009).

Importantly, while traditional Fabry–Perot configurations rely on phases being accumulated purely in the dielectric layer, the presence of lossy mirrors enables nontrivial phases at the interface dielectric-mirror. This relaxes the requirements for the thickness of the dielectric, resulting in an angle-independent resonance for very thin dielectrics. While in conventional FP resonators the angle of incidence is critical, and thus such color schemes display iridescence, our approach

https://doi.org/10.1021/acsphotonics.3c00632
ACS Photonics XXXX, XXX, XXX−XXX

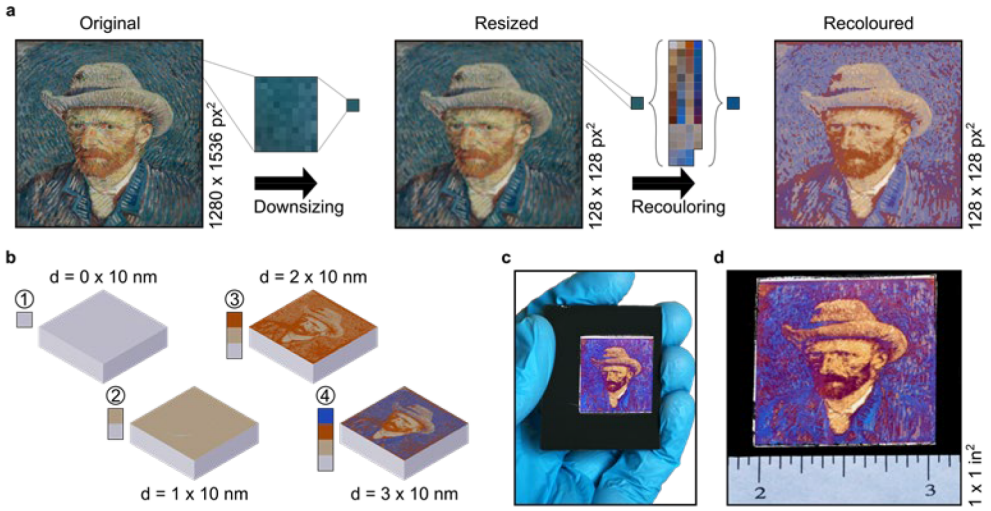

Figure 5. A color reproduction of Van Gogh's self-portrait. (a) To prove the applicability of the approach we target the printing of a colored reproduction of Van Gogh's "Self-portrait with Grey Felt Hat". A MATLAB code takes the original image (left), resizes it to 128 × 128 pixels (center), and recolorizes it with the corresponding nearest color of our expanded color palette (right). (b) As only 4 primaries are used, the entire image can be made by sequentially evaporating 10 nm of TiO_2 on selected areas with three lithographic masks. (c, d) Photography of a 1 × 1 in^2 sample reprinting Van Gogh's paint with colorless colored titanium.

shows great angle-independency. This feature, essential in applications such as colored displays, is further analyzed by measuring in an integrating sphere (RTC-060-SF, Labsphere) coupled to the spectrometer three titanium samples coated with layers of titanium dioxide of 10 nm (yellow), 20 nm (magenta), and 30 nm (cyan), Figure 3g. As can be seen, both the shape and spectral position of the resonances remain constant at angles up to 65°.

Expanding the Color Palette. Although changes in the thickness of the oxide layer result in changes in the color of the structure, this increases the cost of production of colors and is often times impractical. To expand the color space available, we propose a synthesis system similar to that of the RGB displays. In this scheme, only 4 primaries (white, yellow, magenta, and cyan) corresponding to coatings of titanium dioxide of 0 to 30 nm are required to mix and produce a full color palette of 58 hues, Figure 4a. We combine two of the primaries in different proportions by depositing them side-by-side, in a given ratio of total covered area, by using a lithographic mask in a chess-board arrangement, Figure 4b. The subpixels have 100 μm length and a variable width from 0 to 100 μm, while the diagonal arrangement is chosen to avoid color aliasing and produce smooth surfaces. The effective color of any mixture of a two primaries A and B, with reflection curves R_A and R_B, is given by the simple addition rule:

$$R(\alpha) = (1 - \alpha)R_A + \alpha R_B \tag{4}$$

where α is the defined as the ratio of area covered by primary B to the total area $(A + B)$. Although the color pallet can be further enhanced by incorporating multilayers with added fabrication complexities and tolerances, with this simple approach up to 58 colors can be produced out of the original 4 primaries, Figure 4c, thus reducing the costs and significantly improving the viability of the structure in real world applications.

Nanostructural Color Reproduction. Conveniently, as the only difference between the 4 primaries is the thickness of the dioxide layer, the production of an image of up to 58 different colors can be done by evaporating on specific regions of a titanium mirror, 3 sequential layers of 10 nm dioxide, thus producing all 4 primaries with only 3 evaporations. To prove the potential of this technique, we attempt to reproduce Vincent van Gogh's famous "Self-Portrait with Gray Felt Hat", Figure 5a. For that we first resize the original digital picture[48] and then find the closest colors among our expanded color palette to define the three lithographic masks that will be sequentially used to fabricate a reproduction of the painting.

In order to reduce the computational requirements of this proof-of-principle, we start by reducing the original digital picture from a resolution of 1280 × 1536 × 128 × 128 sq. pixels. The color of each of the pixels of the downsized image are obtained by dividing the original picture into 16384 areas of 12 × 10 pixels each and averaging for each section the colors of the constituent pixels. Once the sRGB color of each pixel in the resized image has been determined, we convert from the sRGB coordinates to the CIEXYZ space:

$$\begin{pmatrix} X \\ Y \\ Z \end{pmatrix} = M \begin{pmatrix} R \\ G \\ B \end{pmatrix}$$

with M being the conversion matrix for illuminant given by

$$M = \begin{pmatrix} 0.4361 & 0.3851 & 0.1431 \\ 0.2225 & 0.7169 & 0.0606 \\ 0.0139 & 0.0971 & 0.7148 \end{pmatrix}$$

After the CIEXYZ values are computed, we convert them to CIELAB according to the method explained above.

With the CIELAB values of the resized image computed, we can then associate each of the pixels j of the resized image to the closest color i of our expanded CIELAB color space. The closest color is defined as the color that minimizes the distance:

$$\delta_{ij} = \sqrt{(L_j - L_i)^2 + (a_j - a_i)^2 + (b_j - b_i)^2}$$

https://doi.org/10.1021/acsphotonics.3c00632
ACS Photonics XXXX, XXX, XXX−XXX

The right panel of Figure 5a corresponds to this recolored self-portrait, as digitally recolored in Matlab.

Interestingly, as each of the 58 colors of the expanded color palette is ultimately made by combining two of the primaries, and the primaries can be produced by additive evaporation of up to 3 times 10 nm titanium dioxide layers, we can design three sequential masks that selectively cover areas from further evaporation, thus controlling the white (d = 0 nm), yellow (d = 10 nm), magenta (d = 20 nm), and cyan (d = 30 nm) areas and produce a 58-colored picture in only three evaporations.

The process starts with a clean substrate coated with titanium; the first mask is designed to cover only the areas where the white primary is to be found and expose the rest to be coated with 10 nm of TiO_2. The results of this and subsequent steps are artistically shown in Figure 5b. Then, a second mask designed to cover the yellow and white pixels but expose the rest is employed. After the second evaporation of 10 nm titanium dioxide the sample is ready for the addition of the last 10 nm of oxide. For this third step a mask that is designed to cover the magenta, yellow, and white areas but expose the rest is used. After the last oxide evaporation all four primaries will be in the sample and the image will be reconstructed with the 58 colors of the expanded color space.

Following this fabrication process, we can reproduce Van Gogh's self-portrait. A photograph of this reproduction is found in Figure 5c. We select each of the superpixels that define each of the 58 colors to be made out of 4 by 4 subpixels arranged in the chessboard explained above, see inset of Figure 4b. Therefore, after fabrication, each pixel of the 128 × 128 pixels recolored image is printed on a 0.4 × 0.4 mm^2 area and the total reconstructed portrait spaces over an area of about 2.5 × 2.5 cm^2, demonstrating the applicability of the technique in the preparation of large-scale samples. Indeed, in coloration applications, pixel sizes smaller than the resolution of the human eye (ranging from tens to hundreds of micrometers) do not provide significant advantages. As an example, the state-of-the-art iPhone 14 display pixel dimension is approximately 55 μm.[49]

Finally, although evaporation techniques such as electron beam, sputtering, or atomic layer deposition are currently used in electronics, semiconductors, and optics industries, chemical methods are often preferred for their versatility and scalability. By limiting ourselves to choosing a metal and its oxide, we made the fabrication of the proposed architecture via anodization of a pure metallic layer is made possible. While still further research is required to control the anodization of very thin films, ensuring reproducibility and avoiding chemical contaminants, recent reports have shown promising potential.[50−52] We believe that the use of such chemical methods or other similar approaches can fully leverage these simple nanostructures, enabling their integration into commercial applications.

CONCLUSION

In this work, we report an approach to structural color that relies on an inexpensive subwavelength bilayer Fabry−Perot cavity fabricated from titanium and its oxide. We have studied the optical and material conditions required to produce such a configuration, finding that when transparent lossless dielectrics are used for the cavity layer, losses required to produce near perfect absorption can be introduced by using low-reflection metal materials. Compared to other high-reflection metals, lossy metals such as titanium or chromium result in larger color spaces with more saturated colors. Interestingly, the presence of the lossy mirror introduces nontrivial phases at the dielectric−metal interface that relax the need of phase accumulation at the dielectric and result in angle-independent colors up to 65°.

To demonstrate the applicability of the architecture, we present an expanded color palette that produces 58 different colors from only 4 primaries (white, yellow, magenta, and cyan), by controlling in-plane the ratio of area covered of one of the two primaries with respect to the other in a fashion similar to that of RGB displays. The palette, which can be fully generated with only three sequential evaporations of 10 nm of titanium dioxide (four evaporations in total, including the mirror), can be used to reproduce color images. To prove the versatility and power of this approach, we print a reproduction of the famous Van Gogh's "Self-Portrait with Gray Felt Halt". An algorithm takes the digital picture, reduces its size, and recolors it with the closest colors found in our expanded color palette. These mixed colors, being produced by simple horizontal mixture of four primaries, can be produced by only three lithographic masks in up to three sequential evaporations. With this procedure we reproduce Van Goghs painting on a 1 × 1 in^2 titanium mirror, thus demonstrating the applicability of the design for the production of large-scale images with inexpensive nanostructural colors. Overall, our approach presents a convenient strategy to generate large-scale structural color with low-cost materials (titanium is the ninth most abundant element on Earth) and fully compatible with current industrial fabrication methods, while avoiding the use of toxic contaminants oftentimes present in commercial pigments.

ASSOCIATED CONTENT

Supporting Information

The Supporting Information is available free of charge at https://pubs.acs.org/doi/10.1021/acsphotonics.3c00632.

Additional color palette for low-loss (Al) and high-loss (Cr) mirrors (PDF)

AUTHOR INFORMATION

Corresponding Author

Debashis Chanda − *NanoScience Technology Center, University of Central Florida, Orlando, Florida 32826, United States; Department of Physics, University of Central Florida, Orlando, Florida 32816, United States; CREOL, The College of Optics and Photonics, University of Central Florida, Orlando, Florida 32816, United States*; Email: debashis.chanda@ucf.edu

Authors

Pablo Cencillo-Abad − *NanoScience Technology Center, University of Central Florida, Orlando, Florida 32826, United States*; orcid.org/0000-0002-4118-1560

Sean McCormack − *NanoScience Technology Center, University of Central Florida, Orlando, Florida 32826, United States; CREOL, The College of Optics and Photonics, University of Central Florida, Orlando, Florida 32816, United States*

Tianyi Guo − *NanoScience Technology Center, University of Central Florida, Orlando, Florida 32826, United States*

Aritra Biswas − *NanoScience Technology Center, University of Central Florida, Orlando, Florida 32826, United States;*

https://doi.org/10.1021/acsphotonics.3c00632
ACS Photonics XXXX, XXX, XXX−XXX

CREOL, The College of Optics and Photonics, University of Central Florida, Orlando, Florida 32816, United States

Complete contact information is available at: https://pubs.acs.org/10.1021/acsphotonics.3c00632

Notes

The authors declare no competing financial interest.

■ ACKNOWLEDGMENTS

This work at University of Central Florida was supported by National Science Foundation Grant #ECCS-1920840. P.C.A. acknowledges the support from the UCF Preeminent; Postdoctoral Fellowship Program (P3).

■ REFERENCES

(1) Finlay, V. *Color: A Natural History of the Palette*; Random House, 2007.
(2) Barnett, J. R.; Miller, S.; Pearce, E. Colour and Art: A Brief History of Pigments. *Opt Laser Technol.* **2006**, *38* (4−6), 445−453.
(3) Gregory, P. *High-Technology Applications of Organic Colorants*; Springer: U.S., 1991.
(4) Klein, G. A. *Industrial Color Physics*; Springer Series in Optical Sciences; Springer: New York, NY, 2010; Vol. *154*. DOI: 10.1007/978-1-4419-1197-1.
(5) Mustroph, H. Dyes, General Survey. *Ullmann's Encyclopedia of Industrial Chemistry*; American Cancer Society, 2014; pp 1−38.
(6) Nassau, K. *The Physics and Chemistry of Color: The Fifteen Causes of Color*, 2nd ed.; Wiley, 2001.
(7) Bechtold, T.; Mussak, R. *Handbook of Natural Colorants*; John Wiley and Sons, 2009.
(8) Dushkina, N.; Lakhtakia, A. Structural Colors. In *Engineered Biomimicry*; Elsevier, 2013; pp 267−303.
(9) Cuthill, I. C.; Allen, W. L.; Arbuckle, K.; Caspers, B.; Chaplin, G.; Hauber, M. E.; Hill, G. E.; Jablonski, N. G.; Jiggins, C. D.; Kelber, A.; Mappes, J.; Marshall, J.; Merrill, R.; Osorio, D.; Prum, R.; Roberts, N. W.; Roulin, A.; Rowland, H. M.; Sherratt, T. N.; Skelhorn, J.; Speed, M. P.; Stevens, M.; Stoddard, M. C.; Stuart-Fox, D.; Talas, L.; Tibbetts, E.; Caro, T. The Biology of Color. *Science* **2017**, *357* (6350), na DOI: 10.1126/science.aan0221.
(10) Brillas, E.; Martínez-Huitle, C. A. Decontamination of Wastewaters Containing Synthetic Organic Dyes by Electrochemical Methods. An Updated Review. *Appl. Catal., B* **2015**, *166−167*, 603−643.
(11) Jang, J.; Badloe, T.; Yang, Y.; Lee, T.; Mun, J.; Rho, J. Spectral Modulation through the Hybridization of Mie-Scatterers and Quasi-Guided Mode Resonances: Realizing Full and Gradients of Structural Color. *ACS Nano* **2020**, *14* (11), 15317−15326.
(12) Badloe, T.; Kim, J.; Kim, I.; Kim, W. S.; Kim, W. S.; Kim, Y. K.; Rho, J. Liquid Crystal-Powered Mie Resonators for Electrically Tunable Photorealistic Color Gradients and Dark Blacks. *Light: Science & Applications 2022 11:1* **2022**, *11* (1), 1−11.
(13) Jung, C.; Kim, S. J.; Jang, J.; Ko, J. H.; Kim, D.; Ko, B.; Song, Y. M.; Hong, S. H.; Rho, J. Disordered-Nanoparticle-Based Etalon for Ultrafast Humidity-Responsive Colorimetric Sensors and Anti-Counterfeiting Displays. *Sci. Adv.* **2022**, *8* (10), na.
(14) Jung, C.; Kim, G.; Jeong, M.; Jang, J.; Dong, Z.; Badloe, T.; Yang, J. K. W.; Rho, J. Metasurface-Driven Optically Variable Devices. *Chem. Rev.* **2021**, *121* (21), 13013−13050.
(15) Ko, B.; Badloe, T.; Yang, Y.; Park, J.; Kim, J.; Jeong, H.; Jung, C.; Rho, J. Tunable Metasurfaces via the Humidity Responsive Swelling of Single-Step Imprinted Polyvinyl Alcohol Nanostructures. *Nature Communications 2022 13:1* **2022**, *13* (1), 1−10.
(16) Kinoshita, S; Yoshioka, S; Miyazaki, J Physics of Structural Colors. *Rep. Prog. Phys.* **2008**, *71* (7), 076401.
(17) Kinoshita, S. *Structural Colors in the Realm of Nature*; World Scientific, 2008.
(18) Fu, Y.; Tippets, C. A.; Donev, E. U.; Lopez, R. Structural Colors: From Natural to Artificial Systems. *Wiley Interdiscip Rev. Nanomed Nanobiotechnol* **2016**, *8* (5), 758−775.
(19) Wu, Y.; Chen, Y.; Song, Q.; Xiao, S. Dynamic Structural Colors Based on All-Dielectric Mie Resonators. *Adv. Opt Mater.* **2021**, *9* (11), 2002126.
(20) Toyota Motor Corporation. All-New Lexus LC Structural Blue Edition. https://www.lexus.eu/discover-lexus/lexus-news/lc-structural-blue?lexReferrer=https%3A%2F%2Fwww.google.com%2F#hero (accessed 2022-04-25).
(21) Daqiqeh Rezaei, S.; Dong, Z.; You En Chan, J.; Trisno, J.; Ng, R. J. H.; Ruan, Q.; Qiu, C. W.; Mortensen, N. A.; Yang, J. K. W. Nanophotonic Structural Colors. *ACS Photonics* **2021**, *8* (1), 18−33.
(22) Hu, Q.; Lin, K. te; Lin, H.; Zhang, Y.; Jia, B. Graphene Metapixels for Dynamically Switchable Structural Color. *ACS Nano* **2021**, *15* (5), 8930−8939.
(23) Xuan, Z.; Li, J.; Liu, Q.; Yi, F.; Wang, S.; Lu, W. Artificial Structural Colors and Applications. *Innovation* **2021**, *2* (1), 100081.
(24) Kats, M. A.; Capasso, F. Optical Absorbers Based on Strong Interference in Ultra-Thin Films. *Laser Photon Rev.* **2016**, *10* (5), 735−749.
(25) Born, M.; Wolf, E. *Principles of Optics*; Cambridge University Press, 1999.
(26) Cencillo-Abad, P.; Zheludev, N. I.; Plum, E. Metadevice for Intensity Modulation with Sub-Wavelength Spatial Resolution. *Scientific Reports 2016 6:1* **2016**, *6* (1), 1−7.
(27) Schuller, J. A.; Barnard, E. S.; Cai, W.; Jun, Y. C.; White, J. S.; Brongersma, M. L. Plasmonics for Extreme Light Concentration and Manipulation. *Nature Materials 2010 9:3* **2010**, *9* (3), 193−204.
(28) Kristensen, A.; Yang, J. K. W.; Bozhevolnyi, S. I.; Link, S.; Nordlander, P.; Halas, N. J.; Mortensen, N. A. Plasmonic Colour Generation. *Nat. Rev. Mater.* **2017**, *2* (1), 1−14.
(29) Duan, X.; Kamin, S.; Liu, N. Dynamic Plasmonic Colour Display. *Nature Communications 2017 8:1* **2017**, *8* (1), 1−9.
(30) Song, M.; Wang, D.; Peana, S.; Choudhury, S.; Nyga, P.; Kudyshev, Z. A.; Yu, H.; Boltasseva, A.; Shalaev, V. M.; Kildishev, A. v. Colors with Plasmonic Nanostructures: A Full-Spectrum Review. *Appl. Phys. Rev.* **2019**, *6* (4), 041308.
(31) Zhang, J.; Ou, J. Y.; MacDonald, K. F.; Zheludev, N. I. Optical Response of Plasmonic Relief Meta-Surfaces. *Journal of Optics (United Kingdom)* **2012**, *14* (11), 114002.
(32) Fan, J. R.; Zhu, J.; Wu, W. G.; Huang, Y. Plasmonic Metasurfaces Based on Nanopin-Cavity Resonator for Quantitative Colorimetric Ricin Sensing. *Small* **2017**, *13* (1), 1601710.
(33) Carrillo, S. G.-C.; Trimby, L.; Au, Y.-Y.; Nagareddy, V. K.; Rodriguez-Hernandez, G.; Hosseini, P.; Rios, C.; Bhaskaran, H.; Wright, C. D. A Nonvolatile Phase-Change Metamaterial Color Display. *Adv. Opt Mater.* **2019**, *7* (18), 1801782.
(34) Abdollahramezani, S.; Hemmatyar, O.; Taghinejad, H.; Krasnok, A.; Kiarashinejad, Y.; Zandehshahvar, M.; Alù, A.; Adibi, A. Tunable Nanophotonics Enabled by Chalcogenide Phase-Change Materials. *Nanophotonics* **2020**, *9* (5), 1189−1241.
(35) Zhao, J.; Zhou, Y.; Huo, Y.; Gao, B.; Ma, Y.; Yu, Y. Flexible Dynamic Structural Color Based on an Ultrathin Asymmetric Fabry-Perot Cavity with Phase-Change Material for Temperature Perception. *Optics Express* **2021**, *29* (15), 23273−23281.
(36) Franklin, D.; Chen, Y.; Vazquez-Guardado, A.; Modak, S.; Boroumand, J.; Xu, D.; Wu, S. T.; Chanda, D. Polarization-Independent Actively Tunable Colour Generation on Imprinted Plasmonic Surfaces. *Nature Communications 2015 6:1* **2015**, *6* (1), 1−8.
(37) Cencillo-Abad, P.; Mastranzo-Ortega, P.; Appavoo, D.; Guo, T.; Zhai, L.; Sanchez-Mondragon, J.; Chanda, D. Reusable Structural Colored Nanostructure for Powerless Temperature and Humidity Sensing. *Adv. Opt Mater.* **2023**, na.
(38) Franklin, D.; He, Z.; Mastranzo Ortega, P.; Safaei, A.; Cencillo-Abad, P.; Wu, S.-T.; Chanda, D. Self-Assembled Plasmonics for Angle-Independent Structural Color Displays with Actively Addressed

Black States. *Proc. Natl. Acad. Sci. U. S. A.* **2020**, *117* (24), 13350−13358.
(39) Wang, Q.; Zhang, L.; Cai, X.; Cencillo-Abad, P.; Ou, J.-Y. Tunable Angle-Selective Optical Transparency Induced by Photonic Topological Transition in Dirac Semimetals-Based Hyperbolic Metamaterials. *Optics Express* **2022**, *30* (13), 23102−23114.
(40) Cencillo-Abad, P.; Plum, E.; Rogers, E. T. F.; Zheludev, N. I. Spatial Optical Phase-Modulating Metadevice with Subwavelength Pixelation. *Optics Express* **2016**, *24* (16), 18790−18798.
(41) Scheuer, J. Metasurfaces-Based Holography and Beam Shaping: Engineering the Phase Profile of Light. *Nanophotonics* **2017**, *6* (1), 137−152.
(42) Cencillo-Abad, P.; Franklin, D.; Mastranzo-Ortega, P.; Sanchez-Mondragon, J.; Chanda, D. Ultralight Plasmonic Structural Color Paint. *Sci. Adv.* **2023**, *9* (10), na DOI: 10.1126/sciadv.adf7207.
(43) Pedrotti, F. L.; Pedrotti, L. M.; Pedrotti, L. S. *Introduction to Optics* **2017**, na DOI: 10.1017/9781108552493.
(44) Cencillo-Abad, P.; Ou, J. Y.; Plum, E.; Zheludev, N. I. Electro-Mechanical Light Modulator Based on Controlling the Interaction of Light with a Metasurface. *Scientific Reports 2017 7:1* **2017**, *7* (1), 1−7.
(45) Palik, E. D. *Handbook of Optical Constants of Solids*; Elsevier, 1991.
(46) Yeh, P. *Matrix Formulation for Isotropic Layered Media*; Wiley, 2005.
(47) Rakic, A. D.; Djurišić, A. B.; Elazar, J. M.; Majewski, M. L. Optical Properties of Metallic Films for Vertical-Cavity Optoelectronic Devices. *Applied Optics* **1998**, *37* (22), 5271−5283.
(48) Van Gogh, V. *Self-Portrait with Grey Felt Hat*; Van Gogh Museum, Rights & Reproduction Department, 1887.
(49) *iPhone 14 and iPhone 14 Plus - Technical Specifications - Apple*. https://www.apple.com/iphone-14/specs/ (accessed 2023-06-21).
(50) Siket, C. M.; Tillner, N.; Mardare, A. I.; Reuveny, A.; Grill, C. D.; Hartmann, F.; Kettlgruber, G.; Moser, R.; Kollender, J. P.; Someya, T.; Hassel, A. W.; Kaltenbrunner, M.; Bauer, S. Direct Writing of Anodic Oxides for Plastic Electronics. *npj Flexible Electronics 2018 2:1* **2018**, *2* (1), 1−10.
(51) Sagar, S.; Mohammadian, N.; Park, S.; Majewski, L. A.; Das, B. C. Ultra-Thin Anodized Aluminium Dielectric Films: The Effect of Citric Acid Concentration and Low-Voltage Electronic Applications. *Nanotechnology* **2020**, *31* (25), 255705.
(52) Zhang, F.; Ju, P.; Pan, M.; Zhang, D.; Huang, Y.; Li, G.; Li, X. Self-Healing Mechanisms in Smart Protective Coatings: A Review. *Corros. Sci.* **2018**, *144*, 74−88.

https://doi.org/10.1021/acsphotonics.3c00632
ACS Photonics XXXX, XXX, XXX−XXX